In situ fluorescence/photoacoustic monitoring of diatom algae

J. Cvjetinovic*[a], Yekaterina D. Bedoshvili[b], Daniil V. Nozdriukhin[a,c], Olga I. Efimova[d], Alexey I. Salimon[e], Nadezhda A. Volokitina[b], Alexander M. Korsunsky[e,f], Dmitry A. Gorin[a]

[a]Biophotonics lab, Center for Photonics and Quantum Materials, Skolkovo Institute of Science and Technology, 3 Nobelya Str., Moscow, 121205, Russia
[b]Limnological Institute SB, Russian Academy of Sciences, Ulan-Batorskaya Str., 3, Irkutsk, 664033 Irkutsk
[c]Institute for Biomedical Engineering and Institute of Pharmacology and Toxicology, University of Zurich and ETH Zurich, Switzerland
[d]Center for Neurobiology and Brain Restoration, Skolkovo Institute of Science and Technology, 3 Nobelya Str., Moscow, 121205, Russia
[e]Hierarchically Structured Materials lab, Center for Energy Science and Technology, Skolkovo Institute of Science and Technology, 3 Nobelya Str., Moscow, 121205, Russia
[f]Department of Engineering Science, University of Oxford, Oxford, OX1 3PJ, United Kingdom

ABSTRACT

Photosynthetic single-celled diatom algae, due to their unique structure and properties, represent promising candidates for various applications in technology and biomedicine. These nanostructured objects, enveloped within a silica cell wall called a frustule, play a significant role in Earth's ecology. In this study, we proposed new techniques for monitoring the growth of diatoms—in situ fluorescence measurements using the IVIS imaging system and photoacoustic measurements with a raster scanning optoacoustic mesoscopy (RSOM) setup. Two different diatom cultures, *Achnanthidium sibiricum* and *Encyonema silesiacum*, were cultivated under the optimal conditions in the incubator and monitored over the period of 70 days. Our results showed that the total radiant efficiency increases with increasing incubation time for *E. silesiacum*. Simultaneously, for *A. sibiricum* it slightly decreases after 56 days, indicating that diatoms were at the end of their exponential growth phase. The photoacoustic signal from *E. silesiacum* was lower than from *A. sibiricum*, which is in good agreement with spectroscopic characterization results. The IVIS imaging system made it possible to assess the growth and viability of diatom cells without compromising cell integrity. In contrast, photoacoustic imaging has proved to be suitable for the rapid detection and thorough in situ assessment of the density of diatom colonies due to the presence of light-absorbing chromophores. These methods can be used to monitor the growth of diatoms and facilitate the harvesting of bioactive substances derived from diatoms for pharmaceutical and biomedical purposes.

Keywords: Absorbance, Confocal laser scanning microscopy, Diatoms, Fluorescence imaging, *In vivo* Imaging System (IVIS), Photoacoustic imaging

1. INTRODUCTION

Diatoms are unicellular algae of microscopic size (2–250 μm) with a complex hierarchical porous structure[1]. Diatoms grow in both terrestrial and aquatic habitats and are found in most regions of the world. Since their inception, diatoms have evolved into the largest group of eukaryotic algae with over 100,000 species[2]. They are ecologically important organisms, as their photosynthetic activity is almost equal to that of all tropical forests together. Besides, they produce nearly 20% of the total oxygen and 40% of the annual carbon production in the ocean[3]. Cells are distinguished by the presence of a "shell" called frustule, which is formed by amorphous silicon dioxide. The diatom frustule consists of two intersecting halves: the upper called the epitheca, and the lower, the hypotheca[4], which fit into each other, resembling a Petri dish. There are two groups of diatoms: pennate, with bilateral symmetry, and centric, with radial symmetry[5]. One of

Dynamics and Fluctuations in Biomedical Photonics XVIII, edited by Valery V. Tuchin, Martin J. Leahy
Ruikang K. Wang, Proc. of SPIE Vol. 11641, 116410G · © 2021 SPIE
CCC code: 1605-7422/21/$21 · doi: 10.1117/12.2588254

the main features of diatoms is the unique structure of their cell wall, decorated with pores ranging in size from nano to micrometers. Due to a large number of pores of various sizes, cells have a high specific surface area, high adsorption, and porosity, which can be used for numerous applications[6]. In addition, diatoms find application in various fields due to the possibility of structural changes through genetic manipulation or chemical reactions, high mechanical stability, optical properties such as light focusing and luminescence, biocompatibility, low cost, and toxicity[7].

Researchers have recently begun to discover how these microscopic organisms can improve existing technologies that have beneficial effects on our lives and health. They may find applications in the development of various devices, for example, for water purification and adsorption of heavy metals, for sorting microfluidic particles, as bio- and gas sensors, supercapacitors, batteries, solar cells, electroluminescent devices and drug delivery systems[8–14]. Diatomaceous earth or diatomite, composed of fossilized diatoms, is used in dentistry as an abrasive in toothpaste and as a filler for alginate impression materials since it can improve the strength and stiffness of the alginate gel[15]. Moreover, diatomite produces a smooth texture while ensuring a solid, tack-free gel surface[16]. Purified diatom frustules can be used in regenerative medicine and dentistry applications for enhancing adhesion and proliferation of cells[17–19]. They are also introduced as a cheap and noncytotoxic hemostatic agent for hemorrhage control[20]. Another promising direction is the use of chlorophyll from diatoms as a photosensitizer in photodynamic therapy to treat various infections caused by bacteria and fungi, especially in dental medicine[21–23]. Chlorophyll *a* absorbs energy in the violet-blue and orange-red regions of the spectrum[24–26]. Diatoms also contain chlorophyll *c*, which mainly absorbs blue and red light[24–26], and carotenoids, the main of which is fucoxanthin, which absorbs from the blue-green to yellow-green part of the visible spectrum[24–26]. Accordingly, the possibility of using the diatom chromophores as photoactive components in photodynamic therapy for removing plaque and treating gingivitis is being considered. Recently, it has been shown that microalgal chlorophyll produces reactive oxygen species during laser irradiation, further enhancing the photosensitizing effect and tumor cell apoptosis[27]. To use diatoms for specific biomedical purposes, axenic cultures must be grown efficiently and on a large scale. In addition, an essential aspect is the observation of their growth not only in laboratory conditions but also in the natural environment.

Photoacoustic (optoacoustic) and fluorescence imaging represents a promising tool for visualizing and monitoring the growth of diatom algae. Photoacoustic imaging (PAI) is based on the absorption of light pulses and the acoustic responses that are generated as a result of the fast and uneven thermal expansion of an object[28,29]. PAI is a non-invasive, easy-to-use, and highly sensitive biomedical imaging technique that demonstrates the high contrast of traditional optical imaging with superior ultrasound imaging resolution[30]. Therefore, PAI is widely used for imaging various biomedical systems in both preclinical and clinical studies[31–33]. The signal amplitude is based on the optical absorption coefficient of the biomolecule, which is proportional to the concentration of the absorber[34]. Due to the significant concentration of chromophores, diatoms exhibit a strong photoacoustic effect, excited by a green laser with a wavelength of 532 nm[35,36]. Our group showed that the intensity of the photoacoustic signal increases with the concentration of diatoms in the test volume, which ensures reliable calibration for rapid tests. This makes it possible to visualize and quantitatively study diatom colonies and monitor their growth not only in laboratory conditions and bioreactors but also in their natural environment without complicated sample preparation procedures.

In this study, we investigated two different diatom cultures *Achnanthidium sibiricum* (*A. sibiricum*) and *Encyonema silesiacum* (*E. silesiacum*), isolated from the Baikal Lake by monitoring their growth over 70 days in the incubator using raster scanning optoacoustic mesoscopy (RSOM) approach and IVIS SpectrumCT In vivo Imaging system. To gain a better understanding of the state of diatoms during cultivation and their growth phase, we also carried out absorbance and fluorescence spectroscopy measurements in parallel with photoacoustic and fluorescence imaging. This set of monitoring techniques, as believed, will be further widely used elsewhere in aquaculture and incubator practice to facilitate the harvesting of diatom algae and diatom-derived bioactive substances for pharmaceutical and biomedical purposes.

2. MATERIALS AND METHODS

2.1 Collection, cultivation, and counting of diatom algae cells

Two diatom species, *A. sibiricum* (strain 256) and *E. silesiacum* (strain 459) were isolated from the coastal bottom of Lake Baikal and cultivated in the DM medium[37] at Limnological Institute of the Siberian Branch of the Russian Academy of Science, Irkutsk. The samples were carefully transported for further cultivation and studies in the

Biophotonics laboratory of the Skolkovo Institute of Science and Technology in Moscow in plastic test tubes in November 2020. Further, the obtained diatom cultures were grown in a specially designed incubator in Eppendorf cell culture flasks "T-25" (Helicon, Moscow), with sterile filter caps, which provide the gas exchange between the internal space of the flask and the external environment. Each flask contained approx. 30 mL of DM medium. The cultivation temperature was maintained at about 12 ± 1 °C, while the blue and red light-emitting diodes (LEDs) with a 12:12 day-night cycle promoted the growth of the strains. Before measurements, the flasks were manually shaken to detach the cells from the bottom and keep them in suspension. The experiments lasted 70 days from the moment the diatoms began to grow in the incubator.

To control growth at the beginning of incubation, both studied species were cultivated in microvolume in plates[38]. The cells were grown in the culture plate for four days in five replicates in a volume of 200 μL. All cells in each well were counted within four days using an Axiovert 200 inverted microscope (Carl Zeiss, Germany).

2.2 The diatom algae incubator

The Algae reactor consists of two parts: the control unit, maintaining suitable conditions for diatom algae well-being, and the growth chamber. The entire reactor is powered by a 220V AC, transformed into 12V by two independent power supply units (50W for light controlling and 150W for water cooling system). The control unit consists of two independent circuits: the first to control the day-night regime and light brightness, the second one for thermal regulation placed in the PC case.

A dry-contact time relay (220V supply, 12V regulation) provides the day-night cycle with the ability to set on and off by a day of the week and time of day. In the same circuit, a smooth PWM light power controller with an operating frequency of 10 kHz (which prevents flickering of the lighting) is integrated.

In the thermal regulation circuit, the purified water from the growth chamber is sucked by an impeller pump into a water block located on the 80W Peltier element's cold side. The hot side of the Peltier element is cooled by a maintenance-free liquid cooling system with a peak dissipated power of 250 W. Feedback of the Peltier element and the pump is carried out through continuous temperature monitoring by a thermostatic controller with two sensors at the point where water is sucked into the system and water is released back into the core chamber. This way, the temperature inside the growth chamber could be maintained down to 10°C with high precision.

The control unit is combined with the growth chamber with quick-release connectors on the rear panel: a 3.5 mm jacks for temperature sensors and a 12V DC-DC connector for power supply and control of the lighting system. Two silicone hoses connect the water circuit to the pump and the chilled water block.

The growth chamber is a vessel, the walls of which are insulated with layers of foamed polyethylene to maintain the temperature. Inside the growth chamber, a rack is located, in which the temperature sensors and the inlet and outlet hoses are mounted. Inside this frame, another frame on which the cultural flasks with diatoms are rest. On the top cover of the growth chamber, made of 8mm acrylic (thermal barrier), a lighting system is mounted: two LED strips with LEDs that correspond to the bands of maximum light absorption by chlorophyll (phyto light). The strips are stacked to the aluminum profile, which is both a supporting structure and a radiator, and are directed to the cultural flasks at the bottom. A schematic representation of the incubator is shown in Figure 1.

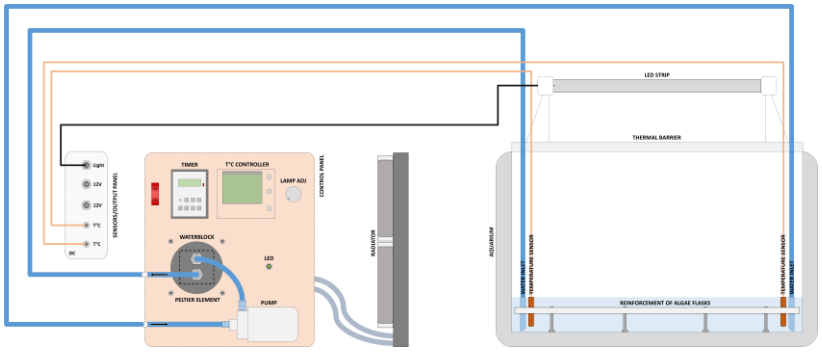

Figure 1. A scheme of the diatom algae incubator

2.3 Scanning electron microscopy

Scanning electron microscopy was used to examine the morphology and size of diatom algae. For that purpose, *A. sibiricum* and *E. silesiacum* diatom cultures were cleaned from organic materials using the following protocol[4]. Firstly, the cells were boiled three times in 6 % SDS (sodium dodecyl sulfate) solution for 30 minutes at 95 °C and washed five times with deionized water. The cell suspension was centrifuged at 1000 × g for 10 min and poured with concentrated nitric acid. The mixture was incubated in a water bath at 95 °C for one hour and then washed three times with ethyl alcohol. After that, the pellets were treated with concentrated hydrochloric acid for 24 h followed by rinsing with water at least five times. The following steps included depositing the purified frustules slurry onto a pre-cleaned crystalline silicon substrate, drying, and mounting on an aluminum stub using a double-sided carbon adhesive tape (SPI, USA). Samples were analyzed without sputter coating. The surface of *A. sibiricum* frustules was imaged with FIB-SEM TESCAN SOLARIS S9251G (Tescan, Czech Republic) at the energy of 1 keV with a Mid-Angle BSE detector. Morphological analysis of *E. silesiacum* cleaned frustules was carried out using a QUANTA 200 electron microscope (FEI, USA) at 30 kV.

2.4 Confocal laser scanning microscopy (CLSM)

The diatom cells were studied by confocal microscopy using Zeiss Axio Observer.Z1 inverted microscope with Plan-Apochromat 40×/1.3 Oil DIC (UV) VIS-IR M27 objective and confocal unit LSM 800 (Carl Zeiss Microscopy GmbH, Germany). The microscope is equipped with four solid-state lasers for illumination of the samples at 405, 488, 561, and 647 nm, three GaAsP PMT detectors, and one T-PMT detector for transmission light detection. Diatoms were imaged using Airyscan detector for higher resolution confocal scanning with appropriate filters. Before measurements, diatoms were stained with DAPI (4′,6-diamidino-2-phenylindole, Sigma Aldrich) to visualize nuclei, according to protocol from[4]. Briefly, the diatom cells were fixed with 4 % formaldehyde for one hour and washed with 0.1 M phosphate buffer (pH 7.4) twice. The cells were collected by centrifugation at 2000 × g for 10 min, followed by DAPI (final concentration, 10 μg/mL) staining. Subsequently, the cells were rinsed twice with the phosphate buffer and mounted using Fluoromount Aqueous Mounting Medium (Sigma Aldrich). DAPI fluorescence was excited with a 405 nm laser, and the emission was registered in the 420-470 nm region. The images were obtained and processed with ZEN 2.3 imaging software.

2.5 Absorbance spectroscopy

The absorbance spectra measurements of *A. sibiricum* and *E. silesiacum* in a 96-well plate were carried out five times from November 27, 2020, to February 1, 2021, using the Infinite M Nano+ dual-mode microplate reader (Tecan Trading AG, Switzerland). The spectra were collected in the wavelength range 400–700 nm with a 2-nm wavelength step at 25 °C.

2.6 Fluorescence spectroscopy

Fluorescence spectra of *A. sibiricum* and *E. silesiacum* diatom suspensions poured in a 96-well plate were recorded with the Infinite M Nano+ by excitation at 450 nm. The emission was observed in the red region (620–750 nm) five times from November 27, 2020, to February 1, 2021.

2.7 Fluorescence measurements with IVIS SpectrumCT In vivo Imaging system

The fluorescence signal from diatoms cultivated in culture flasks was obtained with the IVIS CT Spectrum In Vivo Imaging System (Xenogen Corp., CA, USA). The frame with flasks containing diatom cultures was transferred directly from the incubator to the chamber of the setup for monitoring over fifty days (from December 10, 2020, to January 29, 2021) with excitation/emission at 465/680 nm. The fluorescence signal was quantified using Living Image software (Xenogen Corp., USA). Besides, suspensions of diatoms in a 96-well plate and diatoms mixed with agarose gel were also visualized. To prepare diatom-agarose phantoms, in one case, 3 μL of a diatom suspension was mixed with 7 μL of 1 % agarose gel (A9045-5G, Sigma Aldrich, Germany) and pipetted into a petri dish. In another case, 15 μL of diatoms were mixed with 35 μL of melted agarose. Agarose drop served as a reference sample.

2.8 Raster scanning optoacoustic mesoscopy (RSOM) measurements

The photoacoustic signals from the diatom algae were obtained using RSOM Explorer P50 (iTheraMedical GmbH, Germany). The signal from diatom-agarose gel phantom was excited by a Wedge HB frequency-doubled flashlamp-pumped Nd:YAG laser (Bright Solutions, Pavia, Italy) at an excitation wavelength of 532 nm (repetition rate, 1 kHz; pulse energy, 200 μJ; pulse length, 2.5 ns) and detected with a custom-made spherically focused $LiNbO_3$ detector (center

frequency, 50 MHz; bandwidth, 11–99 MHz; focal diameter, 3 mm; focal distance, 3 mm). The axial and lateral resolution of the RSOM system is 10 μm and 40 μm, respectively. For RSOM imaging, the same samples were used as for IVIS measurements (3 μL of the diatom suspension plus 7 μL 1 % melted agarose for small drops, and 15 μL of the diatoms mixed with 35 μL of agarose for larger drops). The droplets of diatoms embedded in agarose gel were pipetted into a petri dish and after solidification covered with deionized water to ensure coupling between the scan head and the samples. The diatom-agarose phantoms were scanned over a 12 × 12 × 3 mm (6 × 6 × 3 mm) field of view with a raster step size of 20 μm.

3. RESULTS AND DISCUSSION

3.1 Scanning electron microscopy

Diatom cell walls, decorated with a unique pattern of pores and ridges, are shown in Figure 2 by the example of *A. sibiricum* cells. Each frustule has two different valves – hypotheca and epitheca that are connected by several layers of girdle bands. Frustules in girdle view are rectangular and slightly bent around a transapical axis. Linear valves are 7.8–10.5 μm in length and 1.7–2.7 μm wide, ornamented with a row of oblong or slit-like pores called areolae that form parallel and radial striae. Striae are located parallel to the elongated thickening of the valve called costae.

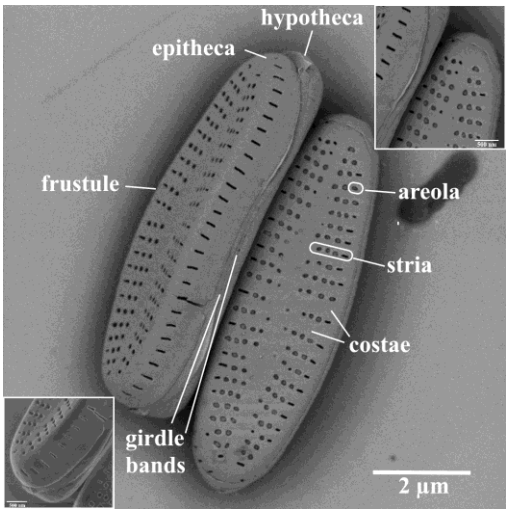

Figure 2. SEM images of *A. sibiricum* showing the basic structure of the cell wall, decorated with pores. Insets: close-up of individual sections of the frustules, scale bar: 500 nm.

A. sibiricum and *E. silesiacum* are both pennate types with bilateral symmetry. The main difference between them is the raphe system. *A. sibiricum* is a monoraphid type of diatoms, whose raphe is present only on one valve of the frustule, as shown in Figure 3a. On the other hand, Figure 3b represents SEM images of *E. silesiacum*, which is asymmetric and biraphid with a raphe on each valve. Valves are dorsiventral, with rounded apices. Their length ranges from 9.8 to 18.7 μm, while the width is 4.5–6.0 μm. Distal raphe ends are curved toward the ventral margin.

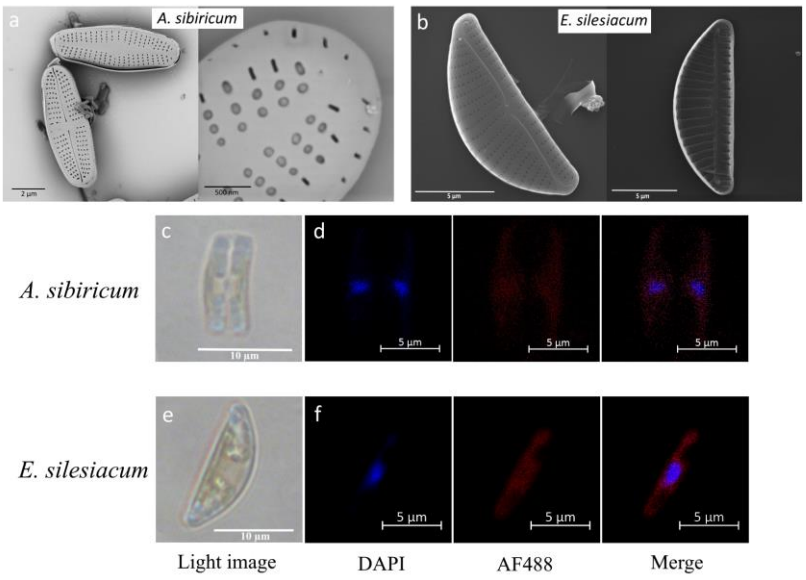

Figure 3. SEM images of: a) *A. sibiricum*, b) *E. silesiacum* frustules; light images of: c) *A. sibiricum*, e) *E. silesiacum* live cells; confocal images of: d) *A. sibiricum*, e) *E. silesiacum* cells fixed formaldexyde and stained with DAPI (blue, nucleus; red, chlorophyll).

3.2 Confocal laser scanning microscopy (CLSM)

We used confocal laser microscopy to observe the DNA material of DAPI-labeled diatom cells. Nuclei of both diatom strains, located in the center of the cells, had an oval shape (Figures 3d, f). The red fluorescence of the chloroplasts was excited with 647 nm wavelength. Chloroplasts occupy most of the cells, which is also confirmed by light images. The state of chloroplasts and cell division indicate the viability of the culture.

3.3 Counting of diatom algae cells in multi-well plastic plates

The growth kinetics of a periodic culture of diatoms is very similar to the growth kinetics of prokaryotic organisms[39]. In this case, the lag phase and the onset of the exponential growth of the culture were observed by cultivating diatoms in microvolumes. Cell counting during the first four days of cultivation showed a steady growth of the culture (Figure 4). After four days of culture, counting was difficult due to the formation of cell clusters. Further growth was more accurately controlled by other proposed methods—fluorescence visualization using IVIS imaging system and photoacoustic measurements with RSOM setup. Since the studied species are benthic (that is, they live on substrates[40]), and capable of secreting a lot of mucus and forming cell clusters[41], the main difficulty in counting cells in microvolume in a well-plate is the impossibility of selecting adequate aliquots and plotting growth curves with sufficiently large technical errors. The proposed methods for assessing chlorophyll, which do not require the extraction of cells from the medium, increase the accuracy of experiments.

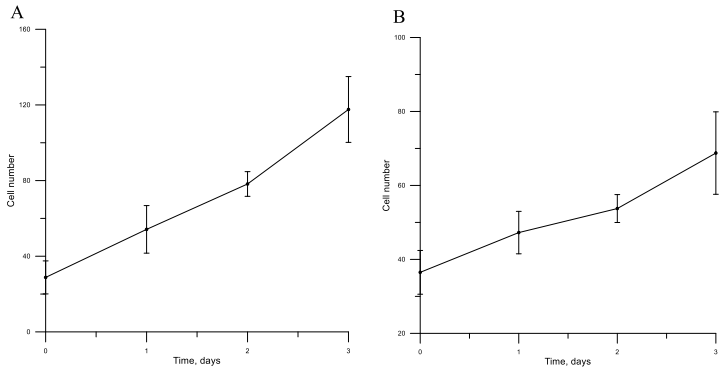

Figure 4. *A. sibiricum* (A) and *E. silesiacum* (B) culture growth during three days after inoculation

3.4 Absorbance spectroscopy

Absorbance spectra of two diatom strains *(A. sibiricum* and *E. silesiacum)* cultured in an incubator for 70 days were measured at different incubation times to track changes in the absorption of light-absorbing pigments (Figure 5). The optical density of *A. sibiricum* (Figure 5a) is increasing with the incubation time up to 56 days. In contrast, the values measured on the 70th day of incubation are lower, indicating the decrease in the concentration of the pigments. The spectra reveal peaks at about 421, 438, and 675 nm, attributable to chlorophyll a[24–26,42]. The bands at 455, 582, and 628 nm were assigned to chlorophyll *c*[24–26,42]. The presence of carotenoid fucoxanthin is represented by a shoulder at about 500 nm[24–26,42]. In the case of *E. silesiacum*, no absorption peaks were observed during the first 20 days of incubation. The peaks could be seen after the first month of cultivation, and they correspond to chlorophyll *a* (at 438 and 674 nm), chlorophyll *c* (at 632 nm), and fucoxanthin (region from 495 to 532 nm). The maximum values were obtained on the 56th day, but they were still lower than for the *A. sibiricum*.

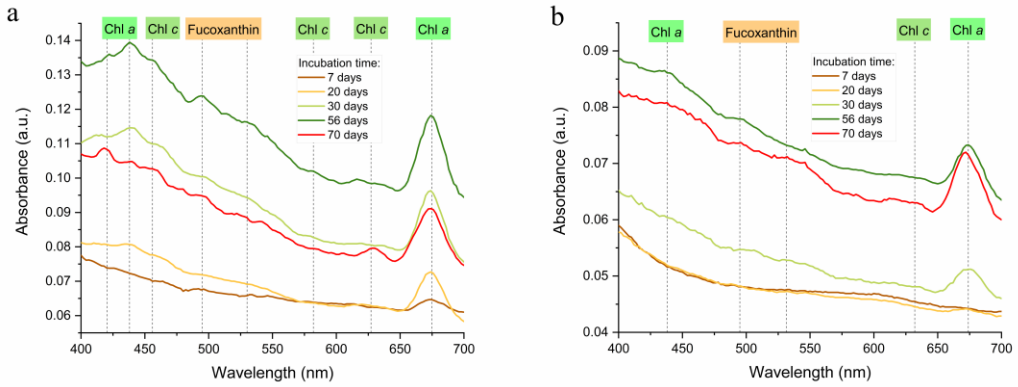

Figure 5. Absorbance spectra of: a) *A. sibiricum*, b) *E. silesiacum*, collected at different periods: 7, 20, 30, 56, and 70 days of incubation.

3.5 Fluorescence spectroscopy

Figure 6 shows the fluorescence intensity spectra of *A. sibiricum* and *E. silesiacum* during the 70 days of cultivation. The spectra were obtained by excitation at 450 nm. All spectra demonstrate an emission band with a maximum at about 682 nm, which corresponds to chlorophyll a[24,42], and a broad shoulder at 715–740 nm. Fluorescence intensity of *A. sibiricum* slowly increases during the cultivation in the incubator (Figure 6a). The maximum values were obtained after 30 days of incubation. In *E. silesiacum* (Figure 6b), the fluorescence intensity increases more evenly with incubation time. Still, the maximum values are almost half as much as in the case of *A. sibiricum* (Figure 6c).

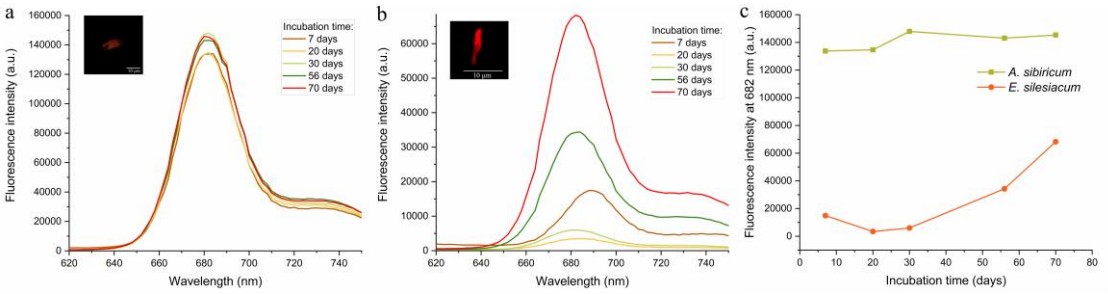

Figure 6. Fluorescence spectra of: a) *A. sibiricum*, b) *E. silesiacum*, collected at different periods: 7, 20, 30, 56, and 70 days of incubation. Insets: Fluorescence images of chlorophyll in cells, scale bar: 10 μm; c) The dependence of fluorescence intensity at 682 nm on the incubation time for both diatom cultures.

3.6 Fluorescence measurements with IVIS SpectrumCT In vivo Imaging system

The results of fluorescence measurements of diatom algae obtained using the IVIS imaging system are presented in Figure 7. The cell culture flasks containing DM medium with diatom cells were transferred directly from the incubator to the IVIS camera for measurements after 20, 39, 56, 63, and 70 days of cultivation. Fluorescence was excited with a 465 nm wavelength, and the emission was registered at 680 nm. It can clearly be seen that the fluorescence intensity is higher for *A. sibiricum*. Total radiant efficiency increases with increasing incubation time. However, in *A. sibiricum* diatoms the maximum values were obtained after 56 days (Figure 7c), which is in good agreement with fluorescence spectra (Figure 7a, c). After that, a slight decrease in values can be observed. The maximum values of total radiant efficiency of *E. silesiacum* are 1.6 times lower than for *A. sibiricum.* By using this method, the growth of diatoms can be monitored quickly and without preliminary sample preparation.

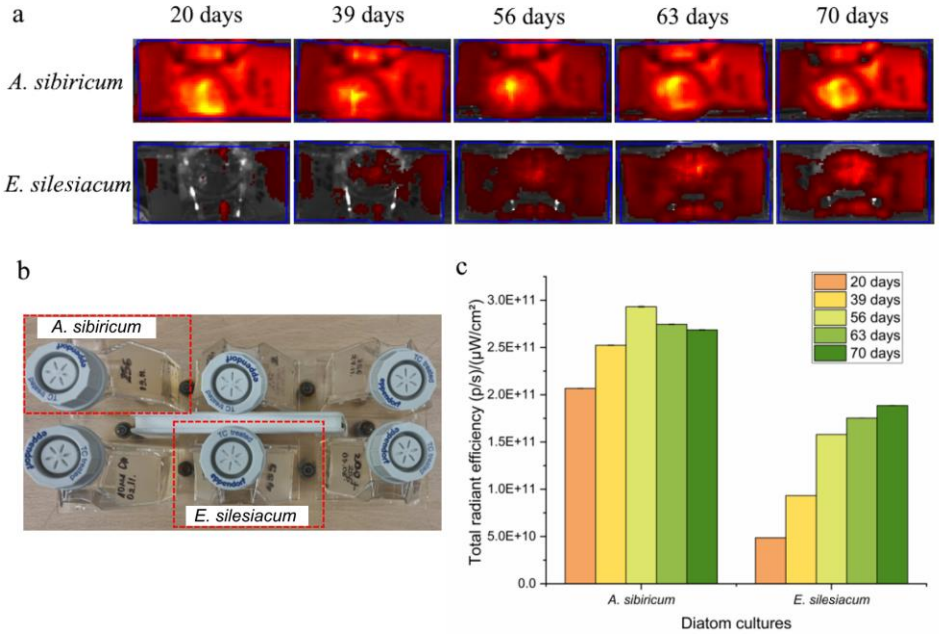

Figure 7. a) IVIS fluorescence images of A. *sibiricum* and *E. silesiacum* in cell culture flasks, b) a photography of cell culture flasks with DM medium and diatoms, c) comparison of total radiant efficiency of both diatom strains during the cultivation period, measured after 20, 39, 56, 63, and 70 days.

3.7 Photoacoustic measurements

The photoacoustic signal from *A. sibiricum* and *E. silesiacum* diatoms excited by 532 nm laser was successfully obtained. Images were processed using ImageJ software by drawing the region of interest and analyzing the color histograms. Figure 8a shows the RSOM images of diatom-agarose droplets received after 30, 56, and 70 days of cultivation. The dependence of the mean pixel intensity signal on the incubation time is represented in Figures 8b, c. The red color indicates a low-frequency signal emitted by larger samples. In contrast, a high-frequency signal, shown with green bars, is emitted by smaller samples. In the case of *A. sibiricum* culture, the highest intensity of the signal emitted by smaller cells is achieved after 30 days of cultivation.

After 56 days, the signal from larger samples is slightly higher, indicating potential aggregation of diatom cells. On the 70th day of incubation, high-frequency signals are practically the same, but a low-frequency signal is lower. On the other hand, photoacoustic signal from *E. silesiacum* is significantly lower, which corresponds to the obtained absorbance spectra (Figure 5b). The maximum signal intensity is obtained after 56 days. The low-intensity signal is higher, which can be explained by the occasional formation of colonies. However, we can observe that the high-frequency signal increases over time. Diatoms embedded in the agarose gel were also visualized using the IVIS imaging system to compare results with RSOM measurements. Figure 8d shows the total radiant efficiency of diatom-agarose droplets and pure agarose droplet after 70 days of incubation.

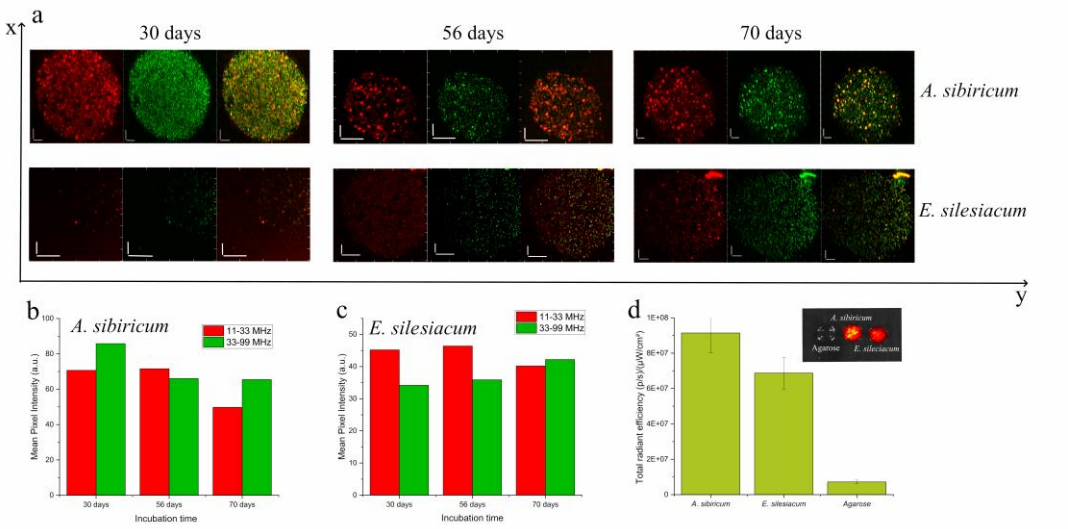

Figure 8. a) RSOM images of *A. sibiricum* and *E. silesiacum* diatoms embedded in agarose gel at 11-33 MHz (red), 33-99 MHz (green), and 11-33 MHz frequencies (merge) after 30, 56, and 70 days of cultivation. Scale bar: x-axis – 0.5 mm, y-axis – 0.5 mm (top left and right corner, bottom right corner), 1 mm (top center, bottom left and center). The dependence of mean pixel intensity on the incubation time of: b) *A. sibiricum*, c) *E. silesiacum*. d) Total radiant efficiency of diatoms mixed with agarose gel obtained using IVIS imaging system. Inset: diatom-agarose droplets compared with pure agarose gel.

In our previous work[35], we discussed in detail the nature of the photoacoustic signal emitted by diatoms. By comparing the absorption at 532 nm and the photoacoustic signal, we concluded that the main light-absorbing pigments found in diatoms, namely chlorophylls *a* and *c* and fucoxanthin, can be considered responsible for the strong photoacoustic effect. The photoacoustic signal induced by light pulses is proportional to the optical energy deposition at the target sample, which is given as the product of the optical absorption coefficient and the local light fluence[43]. According to Beer's law, the absorbance is proportional to the concentration of the absorber. Consequently, the concentration and absorption efficiency of chromophores within the cell walls of diatoms strongly affect the signal intensity. In addition, given the axial and lateral resolution (10 μm and 40 μm, respectively) of the PA microscope, it is impossible to separate individual diatom cells. Besides, the frequencies of signals emitted by diatom cells may be attributed to the eigenfrequencies of vibrating silica frustules[44].

4. CONCLUSIONS

In this study, we investigated two diatom cultures from Lake Baikal—*A. sibiricum* and *E. silesiacum*, cultivated in the incubator and monitored during the 70 days via the IVIS fluorescence imaging and RSOM technique. The obtained results were in good agreement with the fluorescence and absorbance spectra, indicating that diatoms were at the end of the exponential growth phase. The main advantage of the described methods is the ability to quickly assess the growth and viability of cultures for a long time without affecting the integrity of the cells and the inevitable introduction of contamination into the medium during the selection of aliquots. Also, we have established ranges of operating parameters giving robust and verifiable calibration and quantitative assessments. The proposed methods for controlling the growth of diatom cultures expand the possibilities of diatom cultivation and allow the planning of complex experiments without considering the volume of culture for various analyses.

Funding

The collection and cultivation of diatoms were financially supported by the budget project of Limnological Institute, Siberian Branch of the Russian Academy of Sciences # 0279-2021-0008.

Conflict of interest

The authors declare that there are no conflicts of interest.

Acknowledgment

We express our gratitude to Pavel Somov and Elvira Bayramova for providing SEM images of the samples. The IVIS fluorescence imaging, confocal laser scanning microscopy, and RSOM measurements were performed using the equipment of "Bioimaging and Spectroscopy" Core Facility of the Skolkovo Institute of Science and Technology.

REFERENCES

[1] Korsunsky, A. M., Sapozhnikov, P. V., Everaerts, J. and Salimon, A. I., "Nature's neat nanostructuration: The fascinating frustules of diatom algae," Mater. Today **22**(February), 159–160 (2019).

[2] Falciatore, A., Jaubert, M., Bouly, J. P., Bailleul, B. and Mock, T., "Diatom molecular research comes of age: Model species for studying phytoplankton biology and diversity[open]," Plant Cell (2020).

[3] Kale, A. and Karthick, B., "The diatoms," Resonance (2015).

[4] Bedoshvili, Y., Gneusheva, K., Popova, M., Morozov, A. and Likhoshway, Y., "Anomalies in the valve morphogenesis of the centric diatom alga Aulacoseira islandica caused by microtubule inhibitors," Biol. Open **7**(8), 1–10 (2018).

[5] Aitken, Z. H., Luo, S., Reynolds, S. N., Thaulow, C. and Greer, J. R., "Microstructure provides insights into evolutionary design and resilience of Coscinodiscus sp. frustule," Proc. Natl. Acad. Sci. U. S. A. (2016).

[6] Tramontano, C., Chianese, G., Terracciano, M., de Stefano, L. and Rea, I., "Nanostructured biosilica of diatoms: From water world to biomedical applications," Appl. Sci. (2020).

[7] Sprynskyy, M., Pomastowski, P., Hornowska, M., Król, A., Rafińska, K. and Buszewski, B., "Naturally organic functionalized 3D biosilica from diatom microalgae," Mater. Des. (2017).

[8] Uthappa, U. T., Brahmkhatri, V., Sriram, G., Jung, H.-Y., Yu, J., Kurkuri, N., Aminabhavi, T. M., Altalhi, T., Neelgund, G. M. and Kurkuri, M. D., "Nature engineered diatom biosilica as drug delivery systems," J. Control. Release **281**, 70–83 (2018).

[9] Aw, M. S., Simovic, S. and Addai-mensah, J., "Silica microcapsules from diatoms as new carrier for delivery of therapeutics P reliminary C ommunication," 1159–1173.

[10] Janićijević, J., Milić, J., Čalija, B., Micov, A., Stepanović-Petrović, R., Tomić, M., Daković, A., Dobričić, V., Nedić Vasiljević, B. and Krajišnik, D., "Potentiation of the ibuprofen antihyperalgesic effect using inorganically functionalized diatomite," J. Mater. Chem. B **6**(36), 5812–5822 (2018).

[11] Ragni, R., Cicco, S., Vona, D., Leone, G. and Farinola, G. M., "Biosilica from diatoms microalgae: Smart materials from bio-medicine to photonics," J. Mater. Res. (2017).

[12] Rea, I., Terracciano, M. and De Stefano, L., "Synthetic vs Natural: Diatoms Bioderived Porous Materials for the Next Generation of Healthcare Nanodevices," Adv. Healthc. Mater. **6**(3) (2017).

[13] Jeffryes, C., Campbell, J., Li, H., Jiao, J. and Rorrer, G., "The potential of diatom nanobiotechnology for applications in solar cells, batteries, and electroluminescent devices," Energy Environ. Sci. (2011).

[14] Guo, X. L., Kuang, M., Li, F., Liu, X. Y., Zhang, Y. X., Dong, F. and Losic, D., "Engineering of three dimensional (3-D) diatom@TiO2@MnO2 composites with enhanced supercapacitor performance," Electrochim. Acta **190**, 159–167 (2016).

[15] Guiraldo, R. D., Berger, S. B., Consani, R. L. X., Consani, S., De Carvalho, R. V., Lopes, M. B., Meneghel, L. L., Da Silva, F. B. and Sinhoreti, M. A. C., "Characterization of morphology and composition of inorganic fillers in dental alginates," Biomed Res. Int. (2014).

[16] Carlo, H. L., Fonseca, R. B., De Souza Gonçalves, L., Correr-Sobrinho, L., Soares, C. J. and Sinhoreti, M. A. C., "Analysis of filler particle levels and sizes in dental alginates," Mater. Res. (2010).

[17] Cicco, S. R., Vona, D., De Giglio, E., Cometa, S., Mattioli-Belmonte, M., Palumbo, F., Ragni, R. and Farinola, G. M., "Chemically Modified Diatoms Biosilica for Bone Cell Growth with Combined Drug-Delivery and Antioxidant Properties," Chempluschem (2015).

[18] Green, D. W., Lai, W. F. and Jung, H. S., "Evolving marine biomimetics for regenerative dentistry," Mar. Drugs **12**(5), 2877–2912 (2014).

[19] Tamburaci, S. and Tihminlioglu, F., "Diatomite reinforced chitosan composite membrane as potential scaffold for guided bone regeneration," Mater. Sci. Eng. C (2017).

[20] Feng, C., Li, J., Wu, G. S., Mu, Y. Z., Kong, M., Jiang, C. Q., Cheng, X. J., Liu, Y. and Chen, X. G., "Chitosan-Coated Diatom Silica as Hemostatic Agent for Hemorrhage Control," ACS Appl. Mater. Interfaces (2016).

[21] Raghavendra, M., Koregol, A. and Bhola, S., “Photodynamic therapy: A targeted therapy in periodontics,” Aust. Dent. J. (2009).
[22] Abrahamse, H. and Hamblin, M. R., “New photosensitizers for photodynamic therapy,” Biochem. J. (2016).
[23] Kumar, V., Sinha, J., Verma, N., Nayan, K., Saimbi, C. S. and Tripathi, A. K., “Scope of photodynamic therapy in periodontics,” Indian J. Dent. Res. **26**(4), 439–442 (2015).
[24] Kuczynska, P., Jemiola-Rzeminska, M. and Strzalka, K., “Photosynthetic pigments in diatoms,” Mar. Drugs **13**(9), 5847–5881 (2015).
[25] Akimoto, S., Teshigahara, A., Yokono, M., Mimuro, M., Nagao, R. and Tomo, T., “Excitation relaxation dynamics and energy transfer in fucoxanthin- chlorophyll a/c-protein complexes, probed by time-resolved fluorescence,” Biochim. Biophys. Acta - Bioenerg. **1837**(9), 1514–1521 (2014).
[26] Burson, A., Stomp, M., Greenwell, E., Grosse, J. and Huisman, J., “Competition for nutrients and light: testing advances in resource competition with a natural phytoplankton community,” Ecology **99**(5), 1108–1118 (2018).
[27] Qiao, Y., Qiao, Y., Yang, F., Xie, T., Du, Z., Zhong, D., Qi, Y., Li, Y., Li, W., Li, W., Lu, Z., Rao, J., Sun, Y., Sun, Y., Zhou, M., Zhou, M., Zhou, M. and Zhou, M., “Engineered algae: A novel oxygen-generating system for effective treatment of hypoxic cancer,” Sci. Adv. **6**(21) (2020).
[28] Li, C. and Wang, L. V., “Photoacoustic tomography and sensing in biomedicine,” Phys. Med. Biol. **54**(19) (2009).
[29] Manohar, S. and Razansky, D., “Photoacoustics: a historical review,” Adv. Opt. Photonics **8**(4), 586 (2016).
[30] Upputuri, P. K. and Pramanik, M., “Recent advances in photoacoustic contrast agents for in vivo imaging,” Wiley Interdiscip. Rev. Nanomedicine Nanobiotechnology(January), 1–23 (2020).
[31] Wang, L. V. and Hu, S., “Photoacoustic tomography: In vivo imaging from organelles to organs,” Science (80-.). **335**(6075), 1458–1462 (2012).
[32] Karlas, A., Fasoula, N. A., Paul-Yuan, K., Reber, J., Kallmayer, M., Bozhko, D., Seeger, M., Eckstein, H. H., Wildgruber, M. and Ntziachristos, V., “Cardiovascular optoacoustics: From mice to men – A review,” Photoacoustics **14**(March), 19–30 (2019).
[33] Taruttis, A., Van Dam, G. M. and Ntziachristos, V., “Mesoscopic and macroscopic optoacoustic imaging of cancer,” Cancer Res. **75**(8), 1548–1559 (2015).
[34] Tsang, V. T. C., Li, X. and Wong, T. T. W., “A review of endogenous and exogenous contrast agents used in photoacoustic tomography with different sensing configurations,” Sensors (Switzerland) (2020).
[35] Cvjetinovic, J., Salimon, A. I., Novoselova, M. V., Sapozhnikov, P. V., Shirshin, E. A., Yashchenok, A. M., Kalinina, O. Y., Korsunsky, A. M. and Gorin, D. A., “Photoacoustic and fluorescence lifetime imaging of diatoms,” Photoacoustics **18**, 100171 (2020).
[36] Cvjetinovic, J., Salimon, A., Novoselova, M., Sapozhnikov, P., Kalinina, O., Korsunsky, A. and Gorin, D., “Photoacoustic visualization of diatom algae,” Limnol. Freshw. Biol. (2020).
[37] Thompson, A. S., Rhodes, J. C. and Pettman, I., “Culture Collection of Algae and Protozoa: Catalogue of Strains.,” Amblesibe, UK (1998).
[38] Safonova, T. A., Aslamov, I. A., Basharina, T. N., Chenski, A. G., Vereschagin, A. L., Glyzina, O. Y. and Grachev, M. A., “Cultivation and automatic counting of diatom algae cells in multi-well plastic plates,” Diatom Res. (2007).
[39] Sullivan, C. W., “DIATOM MINERALIZATION OF SILICIC ACID. II. REGULATION OF Si (OH)4 TRANSPORT RATES DURING THE CELL CYCLE OF NAVICULA PELLICULOSA,” J. Phycol. (1977).
[40] Kulikovskiy, M., Lange-Bertalot, H., Witkowski, A. and Khursevich, G., “Achnanthidium sibiricum (Bacillariophyceae), a new species from bottom sediments in Lake Baikal,” Arch. Hydrobiol. Suppl. Algol. Stud. **136**(1), 77–87 (2011).
[41] Bedoshvili, Y. D., Gneusheva, K. V., Popova, M. S., Avezova, T. N., Arsentyev, K. Y. and Likhoshway, Y. V., “Frustule morphogenesis of raphid pennate diatom Encyonema ventricosum (Agardh) Grunow,” Protoplasma **255**(3), 911–921 (2018).
[42] Millie, D. F., Schofield, O. M. E., Kirkpatrick, G. J., Johnsen, G. and Evens, T. J., “Using absorbance and fluorescence spectra to discriminate microalgae,” Eur. J. Phycol. **37**(3), 313–322 (2002).
[43] Rajian, J. R., Carson, P. L. and Wang, X., “Quantitative photoacoustic measurement of tissue optical absorption spectrum aided by an optical contrast agent,” Opt. Express (2009).
[44] Abdusatorov, B., Salimon, A. I., Bedoshvili, Y. D., Likhoshway, Y. V. and Korsunsky, A. M., “FEM exploration of the potential of silica diatom frustules for vibrational MEMS applications,” Sensors Actuators, **315** (2020).